Design, Prototyping, and Analysis of a Novel Modular Permanent-Magnet Transverse Flux Disk Generator

Article *in* IEEE Transactions on Magnetics · May 2011

DOI: 10.1109/TMAG.2010.2103365 · Source: IEEE Xplore

4 authors, including:

Javad Moghani
Amirkabir University of Technology
110 PUBLICATIONS **763** CITATIONS

SEE PROFILE

Nima Farrokhzad Ershad
Texas A&M University
22 PUBLICATIONS **280** CITATIONS

SEE PROFILE

Bogi Bech Jensen
University of the Faroe Islands
59 PUBLICATIONS **1,577** CITATIONS

SEE PROFILE

Design, Prototyping, and Analysis of a Novel Modular Permanent Magnet Transverse Flux Disk Generator

Seyedmohsen Hosseini[1], Javad Shokrollahi Moghani[1], Nima Farrokhzad Ershad[1], and Bogi Bech Jensen[2]

[1]Electrical Engineering Department, Amirkabir University of Technology, Tehran 15916, Iran
[2] Centre for Electric Technology, Technical University of Denmark (DTU), Kongens Lyngby, Denmark

This paper presents the design, prototyping, and analysis of a novel modular transverse flux permanent magnet disk generator. The disk-shaped structure simplifies the construction procedure by using laminated steel sheets. To reduce output harmonics, the excitation of the generator is done by circular flat shaped Nd-Fe-B permanent magnets. First, a typical low power generator is designed, and then partially optimized. The optimization objective is to find an inner radius which maximizes the power factor, the output power to mass ratio and the efficiency. The generator equivalent circuit parameters are computed by three dimensional finite element analyses. The simulation results show that the power factor of the proposed structure is considerably greater than the power factor previously reported for other transverse flux permanent magnet generator structures. To verify the simulation results, a prototype has been constructed and tested. The experimental results are in good agreement with simulation results.

***Index Terms*—Disk-shaped structure, finite element analyses, power factor, prototype, transverse flux generator.**

I. Introduction

A transverse flux machine utilizes a magnetic circuit that is in a direction transverse to the direction of motion and the current flow [1]. One of the main advantages of using a transverse flux topology is the possibility to attain a high torque and power density [1], [2]. Nowadays, transverse flux permanent magnet generators (TFPMG) have found great attention for wind power applications [2], [3]. The capability of having large pole numbers, combined with the torque from a TFPMG being almost proportional to the number of poles, makes TFPMGs particularly suitable for gearless wind turbines [3], [4]. As far as the authors know, all previously proposed rotary TFPMGs have a cylindrical structure [5]-[7]. Disadvantages of the cylindrical structures include large inductance, which leads to a lower power factor (*PF*) [8], [9], and construction difficulties related to the use of laminated steel sheets for the construction of the stator cores [10].

This paper presents a novel modular transverse flux permanent magnet disk generator (TFPMDG). A TFPMDG has advantages of having both transverse flux and a disk structure. The disk-shaped profile of a TFPMDG makes it very suitable for use in wind turbines [11], [12]. Also, the disk structure allows high rotational speed due to its ability to counteract centrifugal forces acting on the permanent magnets (PMs). Moreover, construction difficulties caused by using laminated steel sheets are removed in the proposed structure.

In this paper the structure of a TFPMDG is briefly introduced. Secondly, the design process is explained according to which a small power TFPMDG is partially optimized. The optimization objective is to determine a particular inner radius that optimizes the generator performance characteristics. The generator performance characteristics are output power to weight ratio, *PF* and efficiency. In this way, the optimization process needs both magnetostatic and transient three-dimensional finite element analysis (3D FEA) for obtaining the equivalent circuit parameters. To validate the simulation, a prototype TFPMDG has been constructed and tested. The accuracy of the analysis is supported by good agreement between the simulations and test results.

Manuscript received August 21, 2010. Corresponding author: Seyedmohsen Hosseini (e-mail: m_hosseini@aut.ac.ir).
Digital Object Identifier inserted by IEEE

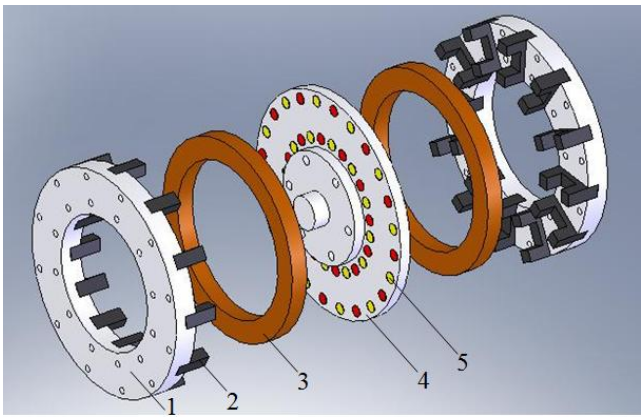

Fig. 1. The structure of the TFPMDG. (1) Stator core holder. (2) Stator core. (3) Armature winding. (4) Rotor Disk. (5) Permanent Magnet.

II. TFPMDG Structure

Fig.1 shows a 3D view of the proposed TFPMDG structure. In this figure, only one phase of the generator is shown, and in order to obtain a three-phase generator, three identical single phase modules (Fig. 1) shifted in space by 120 electrical degrees should be used [5].

Nd-Fe-B rare-earth PMs create the generator excitation. The PMs can be glued into circular holes in the rotor disk. The rotor disk needs to be fabricated from a non-ferromagnetic material, such that the PMs are not magnetically short circuited, and ideally a non-conductive material, such that any eddy current losses induced by harmonics can be eliminated. The stator cores are made from thin steel laminations, inserted

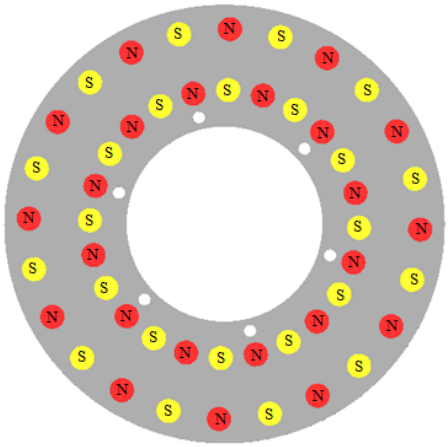

Fig. 2. Arrangements of PMs poles glued into rotor disk in a 12-pole pair TFPMDG.

into machined cavities in the stator core holders. The stator core holders should also have a non-ferromagnetic material, to limit iron losses, and ideally a non-conductive material, such that eddy current losses induced by stray fields from the armature windings can be eliminated. The simple construction and assembly of the lamination steel sheets in the proposed TFPMDG is a great advantage compared to the cylindrical TFPMG structure. It is very difficult to construct the cylindrical TFPMG using laminated steel sheets, which, if eddy current losses are to be limited, can only carry time varying magnetic flux in the plane of the laminations [10]. This problem can be relieved by employing soft magnetic composite cores [13], [14]. However, soft magnetic composite materials have some recognized drawbacks, including lower magnetic permeability and lower saturation flux density, compared to laminated steel sheets. Simply speaking, like-for-like replacement of the laminated steel sheets by soft magnetic composites will result in poorer machine performance [10]. The rotor poles (polarities of the PM's) are shown in Fig. 2. These poles create homopolar fluxes in the stator cores at any time. In the proposed structure, the rotor disk thickness counteracts the centrifugal forces acting on PMs, which makes high speed operation achievable. It should be noted that high rotational speeds are difficult to achieve for cylindrical TFPMGs with an inner rotor [5], [6]. Moreover, since the TFPMDG rotor disk has no ferromagnetic material, the associated rotor core losses are eliminated. If the rotor disk is made of a conductive material there might still be some eddy current losses, due to harmonics. The generator has two armature windings which are located between the stator poles and consist of a simple ring-shaped coil. In the TFPMDG, the number of PMs in one row is twice the number of stator cores on one side. This is necessary if the stator cores are to carry homopolar fluxes. Let p denote the number of pole pairs (which is equal to half of the number of PMs belonging to one row or the number of stator cores in one side) and n *(rps)* denote the rotational speed, then the frequency of the output voltage is exactly determined as for synchronous machines, *i.e.*,

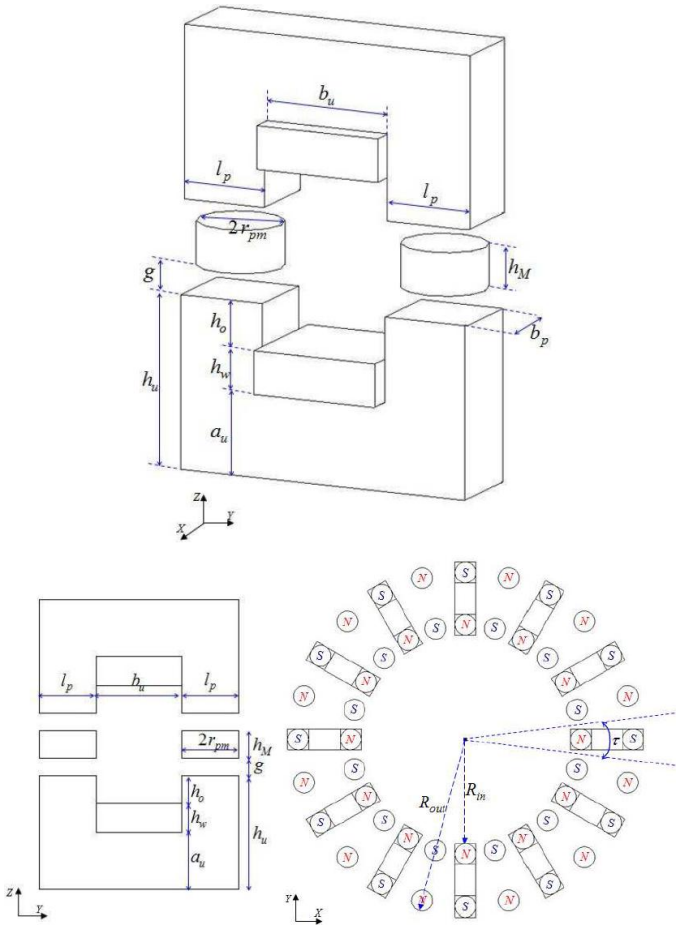

Fig. 3. Dimensions of the TFPMDG in different planes.

$$f = n\,p \tag{1}$$

III. Magnetic Flux and EMF

The first harmonic of the magnetic flux per pole pair per phase excited by the PM rotor is given in [6] as:

$$\Phi_{f1} = \frac{2}{\pi}\tau\, l_p\, B_{mg1}\, k_{area} \tag{2}$$

where $\tau = (R_{out} + R_{in})/p$ is the average pole pitch (in the direction of rotation), l_p is the radial length of the stator pole shoe (Fig. 3), B_{mg1} is the first harmonic of the normal component of the air-gap peak magnetic flux density, and $k_{area} = r_{pm}^2/r_{pm}^2 = \pi/4$ is a coefficient related to the circular cross section of the PMs. R_{out}, R_{in} and r_{pm} are the generator outer radius, generator inner radius and PM radius, respectively (Fig. 3). While the rotor spins at constant speed n, the fundamental harmonic of the magnetic flux is

$$\phi_{f1}(t) = \Phi_{f1}\sin(\omega t) = \frac{2}{\pi}\tau\, l_p\, B_{mg1}\, k_{area}\sin(\omega t) = \frac{2}{\pi}\tau\, l_p\, k_f\, B_{mg}\, k_{area}\sin(\omega t) \tag{3}$$

where $\omega=2\pi f$ is the angular frequency, and B_{mg} is the air-gap magnetic flux density. The form factor $k_f=B_{mg1}/B_{mg}$ of the excitation field depends on the width of stator pole shoe b_p [6]. An approximate value of B_{mg} can be obtained by employing magnetic equation circuit analysis for a pole pair. The instantaneous value of the sinusoidal EMF at no-load induced in N armature turns by the rotor excitation flux ϕ_{f1} is

$$\begin{aligned} e_f &= N\,p\frac{d\phi_{f1}}{dt} = \omega N\,p\,\Phi_{f1}\cos\omega t \\ &= 2\pi f N\,p\,\Phi_{f1}\cos\omega t \end{aligned} \tag{4}$$

The *rms* value of the EMF is

$$\begin{aligned} E_f &= \frac{2\pi}{\sqrt{2}} f N\,p\,\Phi_{f1} \\ &= 2\sqrt{2}\;p^2 N\tau l_p k_f B_{mg} k_{area} n \end{aligned} \tag{5}$$

Hence, by using the EMF constant

$$\begin{aligned} k_E &= \sqrt{2}\pi p^2 N\Phi_{f1} \\ &= 2\sqrt{2}\;p^2 N\tau l_p k_f B_{mg} k_{area} \end{aligned} \tag{6}$$

a simple form of (5) is obtained as below

$$E_f = k_E n \tag{7}$$

IV. Armature Winding Resistance and Reactance

A. Armature winding resistance

The armature winding resistance can approximately be calculated as

$$R_a \approx k_R \frac{N\pi(R_{in}+R_{out})}{\sigma_1 a_w S_a} \tag{8}$$

where k_R is the skin-effect coefficient for resistance, a_w is the number of parallel wires, S_a is the cross section of the armature single conductor, and σ_1 is the conductivity of the armature conductor at a given temperature.

B. Armature winding reactance

The TFPMDG has two ring-shaped armature windings in each phase. Each of these two windings has a self-inductance as well as a mutual inductance with the other winding. The self-inductance of a winding has two components: magnetizing inductance (armature reaction effect inductance) and leakage inductance.

One of the simple methods to calculate the magnetizing inductance is using magnetic equivalent circuits. The magnetic field caused by the armature reaction and the magnetic circuit are depicted in Fig. 4. The d-axis armature inductance is obtained by

$$L_{ad} = \frac{N^2}{4\Re g + 2\Re_{PM}} \tag{9}$$

where $\Re_g$ and $\Re_{PM}$ are the reluctances of one air-gap and one magnet, respectively. For a single pole pair of the generator, the d-axis inductance is therefore

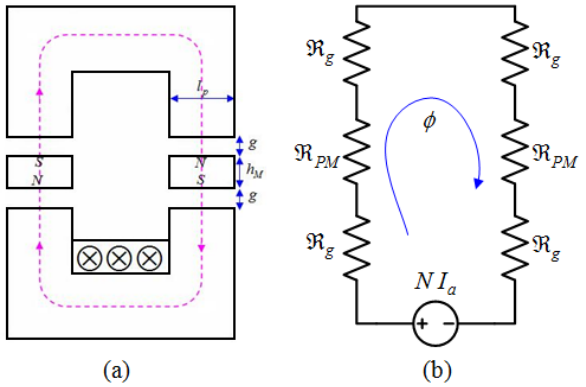

Fig. 4. Calculation of magnetizing inductance. (a) Magnetizing inductance geometry. (b) Magnetic equivalent circuit.

$$L_{ad} = \frac{\mu_\circ N^2 l_p b_p}{4g + \dfrac{2h_M}{\mu_{rrec}}} \tag{10}$$

in which g denotes the mechanical clearance on one side, h_M is the axial length of the PM, and μ_{rrec} is the relative recoil magnetic permeability of the PMs. For a p pole pair generator, (10) should be multiplied by p

$$L_{ad} = p\frac{\mu_\circ N^2 l_p b_p}{4g + \dfrac{2h_M}{\mu_{rrec}}} \tag{11}$$

Similarly, the q-axis armature inductance is determined by

$$L_{aq} = p\frac{\mu_\circ N^2 l_p b_p}{4g + 2h_M} \tag{12}$$

Furthermore, the leakage inductance of the stator winding can be simplified to equal the slot leakage inductance. This is a simplification because it assumes that the flux will only leak straight across the slot and not bulge into the space surrounding the slot. In addition it also assumes that there is no flux around the coil in the sections between the stator cores. The slot leakage inductance consists of the flux that leaks across the slot in the portion occupied by the conductors

$$L_{l1} = 2p\mu_\circ N^2 b_p \frac{h_w}{3b_u} \tag{13}$$

and the flux that leaks across the vacant portion of the slot

$$L_{l2} = 2p\mu_\circ N^2 b_p \frac{h_o}{b_u} \tag{14}$$

where h_w is the axial length of stator slot filled by the conductors, h_o is the axial length of stator slot not filled by the conductors, and b_u is the width of the stator slot (Fig. 3). The leakage inductance, L_l , is therefore

$$L_l = L_{l1} + L_{l2} = 2p\mu_\circ N^2 b_p\left(\frac{h_w}{3b_u} + \frac{h_o}{b_u}\right) \tag{15}$$

From Fig. 4, it's easy to show that the d-axis mutual

inductance, M_d, and q-axis mutual inductance, M_q, are

$$M_d = L_{ad} \quad ; \quad M_q = L_{aq} \tag{16}$$

The synchronous inductances of one phase in the d- and q-axes are the sum of the self inductances and the mutual inductances as

$$L_{sd} = L_{ad} + k_l L_l + M_d = L'_{sd} + M_d \tag{17}$$

$$L_{sd} = L_{aq} + k_l L_l + M_q = L'_{sq} + M_q \tag{18}$$

The L_{sd} and L_{sq} which are estimated analytically from (17) and (18) are not generally the same as those obtained by a 3D FEA. However, for small machines the authors found that more accurate results are obtained if $k_l \approx 3$ in (17) and (18). The synchronous reactances are

$$X_{sd} = X'_{sd} + M_d \omega \ , \ X_{sq} = X'_{sq} + M_q \omega \tag{19}$$

where $X'_{sd} = L'_{sd} \omega$ and $X'_{sq} = L'_{sq} \omega$.

V. Output Power, Efficiency and Power Factor

The per phase equivalent circuit of the TFPMDG is shown in Fig. 5a. It shows that there are two coils per phase and that these have a mutual effect on each other. As the two coils could either be connected in series or parallel they would carry equal currents under normal conditions and Kirchhoff's voltage law would yield

$$\begin{aligned} &\bar{E}_f = jX'_{sd}\bar{I}_{ad} + jX'_{sq}\bar{I}_{aq} + jM_d\omega\bar{I}_{ad} + jM_q\omega\bar{I}_{aq} \\ &+ R_a\bar{I}_a + \bar{V}_{out} = j\left(X'_{sd} + M_d\omega\right)\bar{I}_{ad} + \\ &j\left(X'_{sq} + M_q\omega\right)\bar{I}_{aq} + R_a\bar{I}_a + \bar{V}_{out} = \\ &jX_{sd}\bar{I}_{ad} + jX_{sq}\bar{I}_{aq} + R_a\bar{I}_a + \bar{V}_{out} \end{aligned} \tag{20}$$

where I_{ad} and I_{aq} are the projections of the armature current (load current) I_a on the d- and q-axes, respectively. V_{out} is the output voltage of an armature winding in one phase. Equation (20) states that under balanced conditions, the per phase equivalent circuit of an armature winding is similar to the per phase equivalent circuit of the salient pole synchronous generator (Fig. 5.b). The phasor diagram of an armature winding of the TFPMDG loaded with the resistance (R_L) and reactance (X_L) is depicted in Fig. 6. The associated output voltage projections on the d- and q-axes are

$$\begin{aligned} V_{out}\sin\delta &= I_{aq}\,X_{sq} - R_a\,I_{ad} \\ V_{out}\cos\delta &= E_f - I_{ad}\,X_{sd} - I_{aq}\,R_a \end{aligned} \tag{21}$$

and

$$\begin{aligned} V_{out}\sin\delta &= I_{ad}\,R_L - I_{aq}\,X_L \\ V_{out}\cos\delta &= I_{aq}R_L + I_{ad}\,X_L \end{aligned} \tag{22}$$

where the load angle δ is the angle between the output voltage V_{out} and EMF E_f. Combining (21) and (22), the d- and q-axes currents, independent of the load angle δ, are determined by

$$I_{ad} = \frac{E_f\left(X_{sq} + X_L\right)}{\left(R_L + R_a\right)^2 + \left(X_L + X_{sd}\right)\left(X_{sq} + X_L\right)} \tag{23}$$

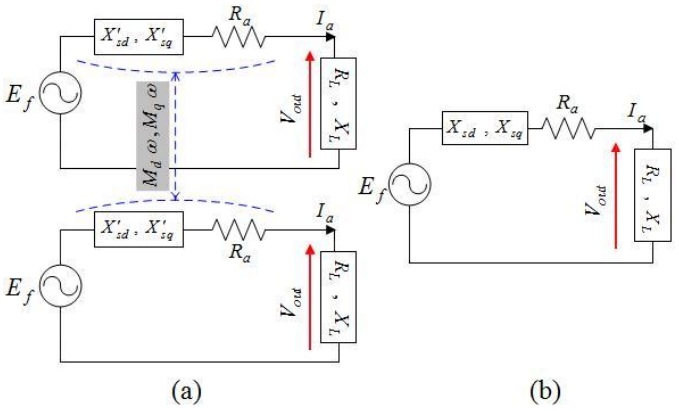

Fig. 5. Equivalent circuit of the TFPMDG (a) Per phase equivalent circuit of the TFPMDG. (b) Per phase equivalent circuit of an armature winding of the TFPMDG.

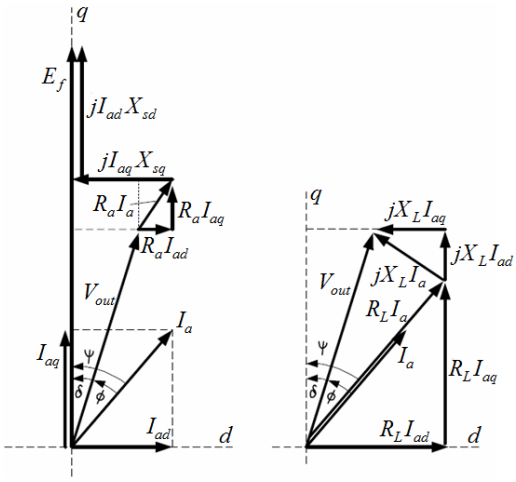

Fig. 6. Phasor diagrams of an armature winding of the TFPMDG loaded with RL load.

$$I_{aq} = \frac{E_f\left(R_L + R_a\right)}{\left(R_L + R_a\right)^2 + \left(X_L + X_{sd}\right)\left(X_{sq} + X_L\right)} \tag{24}$$

where ϕ is the angle between the armature current and output voltage. On the basis of the phasor diagram (Fig. 6) and (21) the output electrical power of an armature winding in one phase of the TFPMDG is

$$P_{out} = E_f\,I_{aq} - I_{ad}\,I_{aq}\left(X_{sd} - X_{sq}\right) - R_a\,I_a^2 \tag{25}$$

The internal electromagnetic power of the generator, P_{elm}, is sum of the stator winding losses, defined by $\Delta P_{lw} = R_a I_a^2$, the stator core losses, defined by ΔP_{lFe}, and the output power, P_{out}. Every phase of the TFPMDG has two armature windings, thus

$$P_{elm} = 2P_{out} + 2\Delta P_{lw} + \Delta P_{lFe} = 2E_f I_{aq} - 2I_{ad} I_{aq} (X_{sd} - X_{sq}) + \Delta P_{lFe} \quad (26)$$

The stator core losses can be calculated if the amplitude and the frequency of the time varying magnetic flux in the stator cores are known. The efficiency of the TFPMDG and power factor (*PF*) are defined as

$$\eta = \frac{2P_{out}}{2P_{out} + 2R_a I_a^2 + \Delta P_{lFe}} \quad (27)$$

$$PF = \frac{E_f - R_a I_{aq}}{V_{out}} \quad (28)$$

when the armature current is chosen to be in phase with the EMF, *i.e.* armature current is in the q-axis direction [7].

VI. Design of a Typical TFPMDG

The aim of this section is to design a typical low power TFPMDG based on the mentioned formulas. Predefined design parameters of the TFPMDG are given in Table I. On the basis of Table I, the output frequency is calculated as $f=n\times p=(2500/60)\times 12=500$Hz. Dimensions of the designed TFPMDG are given in Table II. 48 PMs and 24 stator cores were chosen for the designed TFPMDG. This choice was based on the physical dimensions of the machine, which would be prototyped after the design.

VII. Optimization of the Designed TFPMDG

The optimization goal is to find the inner radius (R_{in} in Fig. 3) that gives the highest output power to active material mass ratio, efficiency and *PF*. The dimensions of the stator lamination pieces and the PM dimensions are kept constant.

TABLE I
PREDEFINED DESIGN PARAMETERS OF THE TFPMDG

Output Power of One Phase (W)	400
Pole Pair Number	12
Rotation Speed (rpm)	2500
Fill Factor, k_{fill}	0.55
Current Density, J (A/mm^2)	4
PM Type	NdFeB35
Output Voltage (V)	50
Number of Parallel Wires, a_w	1
Efficiency (%)	> 90
Maximum Air-Gap Flux Density, B_g (T)	0.9

TABLE II
DIMENSIONS OF THE DESIGNED TFPMDG

h_M (mm)	5
r_{pm} (mm)	5
g (mm)	1
b_u (mm)	15
l_p (mm)	10
a_u (mm)	10
h_u (mm)	20
Armature Turns, N	50
Conductor Diameter, d_{con} (mm)	1.13

The optimization described here is therefore a partial optimization of the entire machine that only focuses on where to place the stator cores and the PMs once their dimensions are chosen for a given pole number. The smallest possible inner radius was constrained by mechanical limits, which required a minimum distance of 1mm between two adjacent PMs. Hence, the minimum value of inner radius is calculated as $(R_{in})_{min}$=38mm. For the optimization purpose, the inner radius R_{in} is increased in incremental steps of 2mm. For all inner radii, the equivalent circuit and the performance characteristics of the generator are calculated. Calculating the equivalent circuit parameters requires 3D FEA (note that the equations derived in sections III and IV were only used for the preliminary design of the machine). By increasing the inner radius, the mass of the copper is increased whilst the mass of the PMs and stator core masses are kept unchanged.

The synchronous inductances are calculated using the modified incremental energy method [15]. Each armature winding has its own self inductance and mutual inductance with the other armature winding. These currents are assigned to the armature windings while finding the inductances

$$(I_{left}, I_{right}) = (\Delta i, \Delta i), (\Delta i, 0), (0, \Delta i) \quad (29)$$

Consequently, in every state, the coenergy is calculated using 3D FEA. In (29), I_{left} is the current in the left armature winding, I_{right} is the current in the right armature winding (Fig. 1), and Δi is the nominal current of a generator armature winding. After calculating the coenergy, the self inductance and the mutual inductance are calculated by

$$L(\theta) = \frac{2W_c(\Delta i, 0, \theta_e)}{(\Delta i)^2} \quad (30)$$

$$M(\theta) = \frac{W_c(\Delta i, \Delta i, \theta_e) - W_c(\Delta i, 0, \theta_e) - W_c(0, \Delta i, \theta_e)}{(\Delta i)^2} \quad (31)$$

in which θ_e is the rotor electrical angle position and W_c is the co-energy. The calculated inductances for different inner radii are given in Table III. Results of Table III are calculated with the assumption that the armature windings have one turn. From Table III, d- and q-axes synchronous inductances with *N=50* turns for every inner radii are given by

$$L_{sd} = (L'_{sd} + M_d) \times 50^2 \quad (32)$$

$$L_{sq} = (L'_{sq} + M_q) \times 50^2 \quad (33)$$

In order to calculate the stator core losses, the magnetic flux density for each inner radius should be calculated. Therefore for each R_{in}, a 3D magnetostatic FEA is performed. After the

TABLE III
RESULTS OF INDUCTANCE CALCULATION FOR DIFFERENT INNER RADII

R_{in}(mm)	$L'_{sd}\times10^{-7}$(H)	$M_d\times10^{-7}$(H)	$L'_{sq}\times10^{-7}$(H)	$M_q\times10^{-7}$(H)
38	4.7024	3.0874	4.6977	3.0826
40	4.7443	3.0894	4.7386	3.0835
42	4.7703	3.0753	4.7633	3.0684
44	4.9304	3.1955	4.9228	3.1876
46	4.9517	3.1798	4.9438	3.1714
48	4.9556	3.1463	4.9467	3.1368
50	5.1216	3.2729	5.1104	3.2624
52	5.1308	3.247	5.12	3.2357
54	5.2792	3.3571	5.268	3.3451

FEA, the magnetic flux density in each node of the meshed area, shown in Fig. 7, is derived. Fig. 8 illustrates the magnetic flux density corresponding to two values of R_{in}, for the meshed area shown in Fig.7. The average value of the maximum flux density, $\overline{B}_m$, is the average of surface nodes which is shown in Fig. 8. Having $\overline{B}_m$ and its variation in frequency determined, it is possible to calculate core losses using the Steinmetz method. $\overline{B}_m$ and core losses ΔP_{lFe} are given in Table IV for different inner radii.

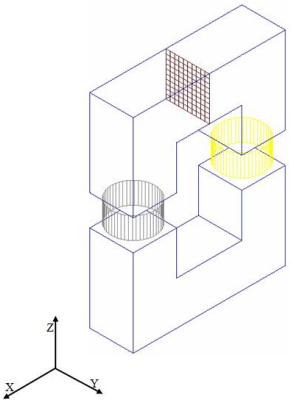

Fig. 7. Meshed area in the stator core.

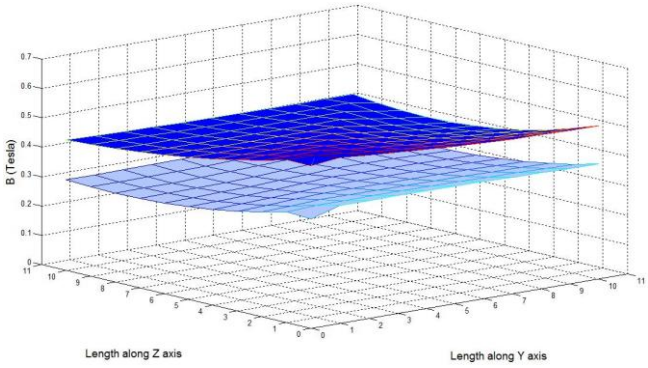

Fig. 8. The magnetic flux density in the meshed area of the stator core. The upper surface is for R_{in}=48 mm and the lower surface is for R_{in}=38mm.

Using 3D transient FEA, the no-load EMF, E_f, in each R_{in} is obtained. In the 3D transient FEA, the rotor is rotated with a fixed speed of 2500rpm. The rotation of the rotor causes a change in the magnetic flux linkage of the armature windings, which induces the armature EMF. Fig. 9 shows the magnetic flux density in the stator cores for R_{in}=38mm at $\theta_e=0^o$. The induced no-load EMFs versus electrical angle are shown in Fig. 10 for the different values of R_{in}. It illustrates that as R_{in} increases, the EMF amplitude increases while its THD decreases. This demonstrates that by increasing R_{in}, pole to pole leakage fluxes decreases. Fourier analysis results of the induced EMFs are given in Table V. It shows that for R_{in} greater than 48 mm, the induced EMF amplitude becomes a constant, and hence that the flux leaking between magnet poles has become insignificant.

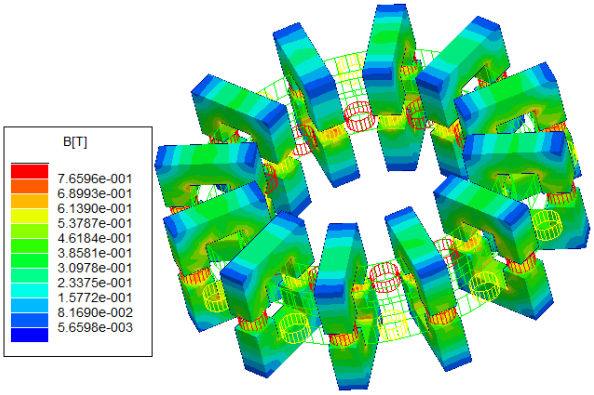

Fig. 9. The magnetic flux density in the stator cores for R_{in}=38mm at $\theta_e=0^0$.

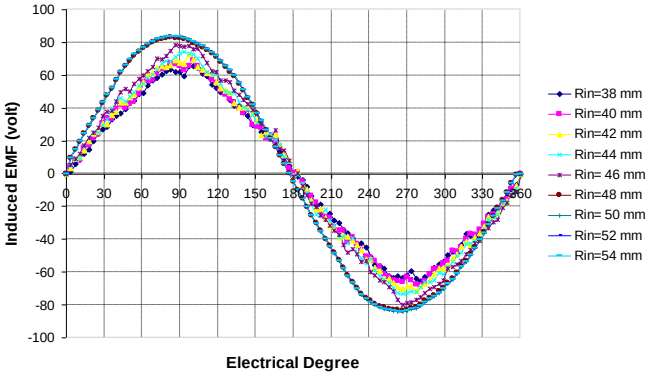

Fig. 10. Induced E_f in the armature winding for different values of R_{in}.

TABLE IV
STATOR CORE LOSSES FOR DIFFERENT INNER RADII

R_{in}(mm)	$\overline{B}_m$ (T)	ΔP_{lFe} (watt)
38	0.31484035	3.50
40	0.33657689	3.85
42	0.36871247	4.24
44	0.39149830	4.49
46	0.42002356	4.82
48	0.43133120	5.01
50	0.43256793	5.11
52	0.43284981	5.18
54	0.43303327	5.23

TABLE V
FOURIER ANALYSIS RESULTS OF THE INDUCED EMFS FOR DIFFERENT INNER RADII

R_{in}(mm)	Fundamental	THD (%)
38	60.54	5.69
40	62.81	5.96
42	65.47	5.90
44	71.65	5.07
46	78.56	4.58
48	83.50	1.85
50	84.01	1.85
52	84.27	1.85
54	84.27	1.85

TABLE VI
GENERATOR PERFORMANCE CHARACTERISTICS FOR DIFFERENT INNER RADII

R_{in}(mm)	P_{out}/Weight (kW/kg)	Efficiency (%)	*PF*
38	0.230217515	96.12	0.8620277
40	0.237162271	96.07	0.8688671
42	0.245515565	96.03	0.8772646
44	0.267246628	96.23	0.8883365
46	0.291454586	96.19	0.9046887
48	0.3078805525	96.50	0.9149688
50	0.3074460863	96.43	0.9104447
52	0.3060857684	96.35	0.9111350
54	0.3037808108	96.27	0.9062084

Having the generator parameters determined in different values of R_{in}, the output power to active material (PMs + stator cores + copper) mass ratio, efficiency and *PF* are calculated. It is assumed that I_{aq}=4A and I_{ad}=0. The Results are given in Table VI which gives the optimized inner radius value as R_{in}=48mm.

The *PF* of the optimized TFPMDG is considerably greater than the *PF* of previously reported TFPMG [5], [7], [9]. The highest previously reported *PF* was 0.62 [7].

VIII. PROTOTYPING AND TESTING OF THE DESIGNED TFPMDG

Because the three phases of the generator are identical, only a single phase of the TFPMDG was prototyped. The procedure of prototyping is summarized in steps below:

(a) Construction of the aluminum rotor disk and gluing the PMs into its holes (Fig. 11), (b) Construction of the aluminum stator core holder and inserting the stator cores into the machined cavities (Fig. 12), (c) Construction of two armature winding (Fig. 13), (d) Assembling of the generator.

The constructed TFPMDG coupled to a DC motor is shown in Fig. 14. Experiments on the TFPMDG are of two types; no load and load tests. In the latter case, a resistive load is used. Fig. 15 shows the no-load voltage waveform and the loaded current waveform at 2500 rpm.

Fig. 11. Rotor Disk with circular flat shaped PMs.

Fig. 12. Inserting the stator cores into the machined cavities of the stator holder.

Fig. 13. Two ring-shaped armature windings.

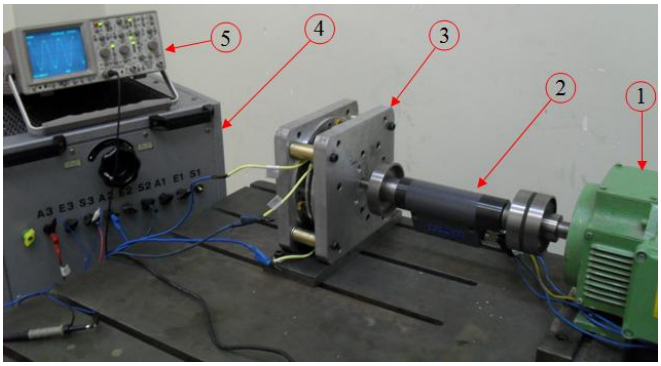

Fig. 14. Test setup. (1) DC motor. (2) Torque meter. (3) Constructed TFPMDG. (4) Resistive load. (5) Oscilloscope.

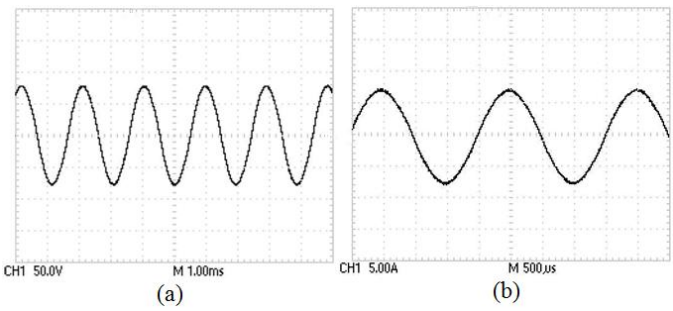

Fig. 15. Output waveforms at 2500rpm. (a) No load voltage. (b) Current waveform with 8 Ω resistive load.

As it can be seen from Fig. 15, that outputs have very low harmonics (THD< 2%) resulting in nearly perfect sinusoidal waveforms. One reason for this is that circular flat shaped magnets were used. The rotational losses, ΔP_{rot}, at 2500 rpm were measured to be 20W. Fig. 16 shows the variation of the output voltage versus load current. Fig. 17 illustrates the output power of one module versus the load current. In Fig. 18, the variation of efficiency versus load current is depicted. It should be noted that the rotational losses, ΔP_{rot}, are taken into account in Figs. 17 and 18. The experimental characteristics of the prototyped TFPMDG are summarized in Table VII. By increasing the load current from its nominal value (4A), the differences between the simulations and the experimental results becomes greater. The simulation results and the experimental results are thus in good agreement up to the nominal current. If the current is increased beyond this value, then the errors become more significant. The major contributors to the discrepancies between the simulations and the experimental results are as follows: (a) weakening of the PMs; dissimilarity between the no-load voltages obtained from the 3D FEA and the experimentally measured no-load voltage (Fig.16 for I_a=0) confirms the weakening of the PMs. (b) Omission of the thermally increased armature resistance in the simulations, as the armature current increases beyond the nominal value. (c) Omission of the conductive aluminum structure in the 3D FEA simulation, which would have some eddy current losses. The omission of the aluminum structure in the simulations is not believed to have had a great impact, since no noticeable temperature increase was detected in neither the rotor disk nor the stator holders.

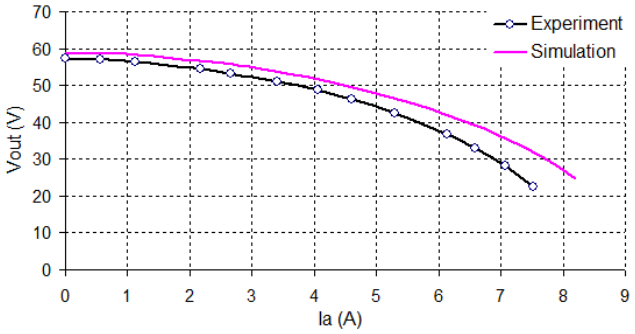

Fig. 16. Variation of output voltage versus load current.

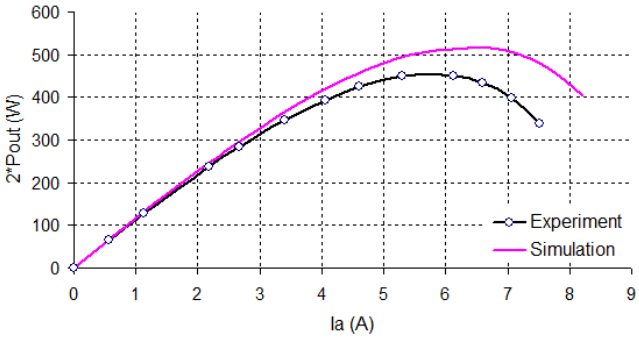

Fig. 17. Variation of output power of one module versus load current.

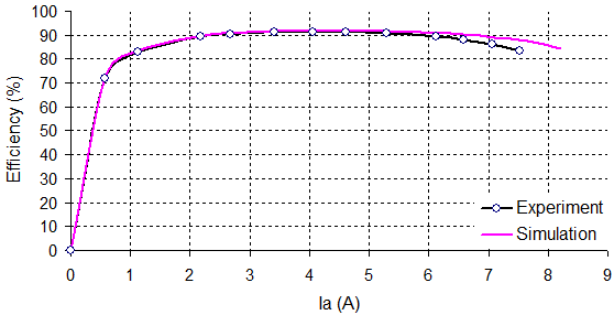

Fig. 18. Variation of efficiency versus load current.

TABLE VII
NOMINAL CHARACTERISTICS OF THE CONSTRUCTED TFPMDG

Load current, I_a (A)	4
Output power of one module, $2P_{out}$ (W)	400
Efficiency (%)	≈ 90
PF	0.8985
Output power/active mass (kW/kg)	0.298
Active outer diameter of one module (mm)	166
Active inner diameter of one module (mm)	96
Active thickness of one module (mm)	47
Output power/Volume (kW/m^3)	591
R_a (Ω)	0.38
X_{sd} (Ω)	6.824
X_{sq} (Ω)	6.808
Output frequency (Hz)	500

IX. CONCLUSION

In this paper, a novel structure of a transverse flux permanent magnet generator was introduced. The proposed structure benefits from the advantageous features of the transverse flux machine as well as disk machine. The disk-shaped profile allows for high rotational speeds and simplifies the construction by using laminated steel sheets. The paper also presents the design procedure of a TFPMDG. A typical low power TFPMDG was designed and partially optimized. The objective of the optimization was to find a possible inner radius which maximizes the output power to mass ratio, the efficiency and the *PF*. The optimization process requires both a 3D magnetostatic FEA and a 3D transient FEA. To validate the simulation a prototyped TFPMDG has been manufactured and tested. Using circular flat-shaped PMs leads to a sinusoidal output, in both voltage and current. The simulations and experimental results show that the *PF* of the TFPMDG is considerably greater than the *PF* of previously reported rotary TFPMG structures. For load currents under nominal value (4 A) there is good agreement between the simulations and the experimental results. As the load current increases beyond the nominal value, the discrepancies between the simulations and the experimental results become greater. One of the major reasons for these discrepancies that the PMs used in the experimental setup were weaker than those used in the simulations, and that the simulations did not include the aluminum structures, which would have some eddy current losses. Additionally, as the load current increases the temperature of the armature winding increases, causing the armature resistance to increase. This was not accounted for

during the simulations.

The disk-shaped profile lead to a very simple transverse flux machine construction, whit laminated steel sheets, low output harmonics and a high *PF*. It can thus be concluded that if the TFPMDG structure can be scaled up to a large version, the TFPMDG could be advantageous in wind power systems.

REFERENCES

[1] H. Weh, H. Hoffmann, and J. Landrath, "New Permanent Magnet Excited Synchronous Machine with High Efficinecy at Low Speeds," in *Proc. Int. Conf. Electrical machines*, Pisa, Italy, 1990, vol. 3, pp. 35-40.

[2] D. Svechkarenko, *On Analytical Modeling and Design of a Novel Transverse Flux Generator for Offshore Wind Turbines*, Licentiate Thesis, Royal Institute of Technology, Stockholm, Sweden, 2007.

[3] P. Lampola, *Directly Driven, Low-Speed Permanent-Magnet Generators for Wind Power Applications*, Ph.D. dissertation, Helsinki University of Technology, Helsinki, Finland, 2000.

[4] M. R. Dubois, *Optimized Permanent Magnet Generator Topologies for Direct Drive Wind Turbines*, Ph.D. dissertation, Delft University of Technology, Delft, The Netherlands, 2004.

[5] J. F. Gieras, "Performance Characteristics of a Permanent Magnet Transverse Flux Generator," in *Proc. IEEE International Conference on Electric Machines and Drives*, San Antonio, USA, 15 May 2005, pp. 1293-1299.

[6] J. F. Gieras, and M. Wing, *Permanent Magnet Motor Technology: Design and Application*, 2rd ed., Marcel Dekker Inc., New York, 2002.

[7] D. Svechkarenko, J. Soulard, and C. Sadarangani, "Performance Evaluation of a Novel Transverse Flux Generator with 3D Finite Element Analysis," in *Proc. Int. Conf. on Electrical Machines and Systems, ICEMS2009*, Tokyo, Japan, 15-18 November 2009, pp. 1-6.

[8] G. Patterson, T. Koseki, Y. Aoyama, and K. Sako, "Simple Modeling and Prototype Experiments for a New High-Thrust, Low-Speed Permanent Magnet Disk Motor," in *Proc. ICEMS2009*, Tokyo, Japan, 15-18 November 2009, pp. 1-6.

[9] M. R. Harris, G. H. Pajooman, and S. M. Abu Sharkh, "The Problem of Power Factor in VPRM (transverse-flux) Machines," in *Proc. IEE Colloq. Electtr. Machines Drives*, 1997, pp.386-390.

[10] Y. Guo, J. G. Zhu, P. A. Watterson, and W. Wu, "Development of a PM Transverse Flux Motor With Soft Magnetic Composite Core," *IEEE Transaction on Energy Conversion*, vol. 21, No.2, pp. 426-434, June 2006.

[11] S. M. Hosseini, M. Agha-Mirsalim, and M. Mirzaei, "Design, Prototyping, and Analysis of a Low Cost Axial-Flux Coreless Permanent-Magnet Generator," *IEEE Transaction on Magnetics*, vol. 44, No. 1, pp. 75-80, January 2008.

[12] J. F. Gieras, R. J. Wang, and M. J. Kamper, *Axial Flux Permanent Magnet Brushless Machines*, Norwell, MA: Kluwer, 2004.

[13] J. Y. Lee, J. W. Kim, J. H. Chang, S. U. Chung, D. H. Kang, and J. P. Hong, "Determination of Parameters Considering Magnetic Nonlinearity in Solid Core Transverse Flux Linear Motor for Dynamic Simulation," *IEEE Transaction on Magnetics*, vol. 44, No. 6, pp. 1566-1568, June 2008.

[14] J. Y. Lee, J. H. Chang, D. H. Kang, S. I. Kim, and J. P. Hong, "Tooth Shape Optimization for Cogging Torque Reduction of Transverse Flux Rotary Motor Using Design of Experiment and Response Surface Methodology," *IEEE Transaction on Magnetics*, vol. 43, No. 4, pp. 1817-1820, April 2007.

[15] M. Gyimesi and D. Ostergaard, "Inductance Computation by Incremental Finite Element Analysis," *IEEE Transaction on Magnetics*, vol. 35, No. 3, pp. 1119-1122, May 1999.

Seyedmohsen Hosseini was born in Tehran, Iran, in 1982. He received the B.S. degree in electrical engineering from Mashhad University, Mashhad, Iran, in 2004 and the M.S. degree in electrical power engineering from Amirkabir University of Technology, Tehran, Iran, in 2006. He is pursuing his Ph.D. program in the Department of Electrical Engineering at Amirkabir University of Technology, Tehran, Iran. Currently, He is working as a visiting researcher at the Centre for Electric Technology, Technical University of Denmark (DTU), Kongens Lyngby, Denmark. In particular, his research interests are numerical and analytical analysis of electromagnetic fields, PM machines, and power electronics.

Javad Shokrollahi Moghani was born in Tabriz, Iran in 1956. He received the BSc and MSc degrees in electrical engineering from the South Bank Polytechnic and Loughborough University of Technology, England, in 1982 and 1984 respectively. Since 1984 until 1991 he was with the Department of Electrical Engineering, Amirkabir University of Technology, Tehran, Iran. He received his PhD degree in electrical engineering from Bath University, Bath, England in 1995 and is back to Amirkabir University of Technology since. His research interests include Electromagnetic System Modeling and Design using FEM, DC-DC converters and Electric Drives.

Nima Farrokhzad Ershad was born in Tehran, Iran, on June 12, 1982. He received his B.S. and M.S. degrees in electrical engineering from Shahed University of Tehran, Tehran, Iran, on 2005 and Amirkabir University of Technology, Tehran, Iran on 2009 respectively. His main interests are analysis, design and manufacturing of electrical machines.

Bogi Bech Jensen was born in the Faroe Islands on November 3rd 1977 and received the Ph.D. degree from Newcastle University, Newcastle upon Tyne, United Kingdom, in 2010 for his research on toroidally wound induction machines. He spent the years from 1994 to 2002 in the marine sector with roles from Engineering Cadet to Senior Field Engineer. He joined academia in 2002 as a Lecturer at the Centre of Maritime Studies and Engineering, Faroe Islands, and was a Research Associate and later a Lecturer at Newcastle University, Newcastle upon Tyne, United Kingdom, during the years from 2007 until 2010. He is currently Associate Professor of Electrical Machines at the Centre for Electric Technology, Technical University of Denmark (DTU), Kongens Lyngby, Denmark.